Turbulence Structure of the Hurricane Boundary Layer between the Outer Rainbands

JUN A. ZHANG

Rosenstiel School of Marine and Atmospheric Science, University of Miami, and NOAA/Atlantic Oceanographic and Meteorological Laboratory/Hurricane Research Division, Miami, Florida

WILLIAM M. DRENNAN

Rosenstiel School of Marine and Atmospheric Science, University of Miami, Miami, Florida

PETER G. BLACK

NOAA/Atlantic Oceanographic and Meteorological Laboratory/Hurricane Research Division, Miami, Florida, and Science Applications International Corporation at Naval Research Laboratory, Monterey, California

JEFFREY R. FRENCH

Department of Atmospheric Science, University of Wyoming, Laramie, Wyoming

(Manuscript received 17 September 2008, in final form 3 February 2009)

ABSTRACT

As part of the Coupled Boundary Layers Air–Sea Transfer (CBLAST)-Hurricane program, flights were conducted to directly measure turbulent fluxes and turbulence properties in the high-wind boundary layer of hurricanes between the outer rainbands. For the first time, vertical profiles of normalized momentum fluxes, sensible heat and humidity fluxes, and variances of three-dimensional wind velocities and specific humidity are presented for the hurricane boundary layer with surface wind speeds ranging from 20 to 30 m s^{-1}. The turbulent kinetic energy budget is estimated, indicating that the shear production and dissipation are the major source and sink terms, respectively. The imbalance in the turbulent kinetic energy budget indicates that the unmeasured terms, such as horizontal advection, may be important in hurricane boundary layer structure and dynamics. Finally, the thermodynamic boundary layer height, estimated based on the virtual potential temperature profiles, is roughly half of the boundary layer height estimated from the momentum flux profiles. The latter height where momentum and humidity fluxes tend to vanish is close to that of the inflow layer and also of the maximum in the tangential velocity profiles.

1. Introduction

Tropical cyclones interact with the ocean through the boundary layer, obtaining heat and moisture and transferring momentum to the ocean in the form of currents and waves. An improved knowledge of the mechanisms underlying air–sea exchange across the boundary layer is essential for interpreting physical, dynamical, and thermodynamical processes, and hence for the development of models with realistic prognostic capabilities for forecasting or simulating tropical cyclones (Emanuel 1995; Braun and Tao 2000; Kepert 2006; Chen et al. 2007; Smith et al. 2008). However, the boundary layer remains the least well-observed part of tropical cyclones. This lack of in situ measurements is due, in large part, to the difficulty of aircraft to penetrate the hurricane boundary layer because of the increased risk associated with flying low in such severe conditions.

Prior to 2003 there were few direct measurements of turbulence in the boundary layer of hurricanes or tropical storms. Moss and Merceret (1976, 1977) and Moss (1978) conducted one stepped descent in the boundary layer of the periphery of 1975 Tropical Storm Eloise, measuring momentum fluxes at different levels. There have since been measurements of hurricane boundary layer structure by airborne radars (Powell 1990a,b) and coastal radars (Wurman and Winslow 1998; Morrison

Corresponding author address: Jun Zhang, NOAA/AOML/Hurricane Research Division, 4301 Rickenbacker Causeway, Miami, FL 33149.
E-mail: jun.zhang@noaa.gov

DOI: 10.1175/2009JAS2954.1

© 2009 American Meteorological Society

et al. 2005), but the radars do not resolve the smaller scales of the velocity field that support most of the stress.

The Coupled Boundary Layers Air–Sea Transfer (CBLAST) experiment provided a unique dataset that includes measurements of the vertical structure of turbulence throughout the hurricane boundary layer between the outer rainbands (Black et al. 2007). Drennan et al. (2007) and French et al. (2007) reported the first direct measurements of momentum and humidity fluxes in the high-wind hurricane boundary layer with surface wind speeds up to 30 m s^{-1} using data collected in Hurricanes Fabian (2003) and Isabel (2003). Zhang et al. (2008) reported sensible heat and enthalpy fluxes from the same experiment. Here we present the turbulence statistics for the hurricane boundary layer between the outer rainbands using CBLAST data collected in four hurricanes in 2003 and 2004.

In the next section, we give a brief description of the experiment and data. In sections 3 and 4, we present the vertical structure of turbulent fluxes and turbulence properties, respectively. The turbulent kinetic energy (TKE) budget is presented in section 5, followed by a discussion and conclusions in section 6.

2. Description of the experiment and data

Major field campaigns for the CBLAST experiment were conducted during the Atlantic hurricane seasons of 2003 and 2004. Black et al. (2007) provide a detailed summary of the experiment; here we present details relevant to the present study. As part of CBLAST, measurements of turbulence and other quantities were obtained by a specially instrumented National Oceanic and Atmospheric Administration (NOAA) WP-3D Orion aircraft (N43RF, hereafter NOAA-43). Typical flights lasted about eight hours and included separate modules designed to study eyewall structure and dynamics, and boundary layer processes. The boundary layer module consisted of along- and crosswind stepped descents with a series of legs roughly 30 km in length at altitudes from 800 m to as low as 60 m above the sea surface. The stepped descents were conducted in clear-air regions between rainbands or away from rainbands, as dictated by flight safety concerns. Because of operational constraints, the descents were not stacked but carried out in linear fashion. Details of the modules related to storm position and motion are discussed by Drennan et al. (2007) and Black et al. (2007).

The three-dimensional wind vector was measured using two independent systems. The first system uses fuselage-mounted Rosemount 858Y sensors for attack and sideslip angles, and separate sensors for static and dynamic pressure. The second system uses a 9-hole ''Best Aircraft Turbulence'' (BAT) probe system installed at the end of a 2-m boom in front of the nose. In all cases, the velocity data are corrected for aircraft motion, measured with an inertial navigation system and global positioning system (GPS). Descriptions of the instrumentation, calibration, and motion corrections are given by French et al. (2007). Fast response humidity data were obtained using a modified (LI-COR) LI-7500 infrared gas analyzer installed in the radome (Drennan et al. 2007). Temperature was measured using a fast response (130 μm) Rosemount 102a thermistor, as discussed by Friehe and Khelif (1992) and Khelif et al. (1999).

GPS dropsondes launched from another NOAA P3 aircraft, N42RF, in the vicinity of NOAA-43 provided profiles of wind speed, temperature, and humidity from flight levels down to the surface. The vertical resolution of the wind and thermodynamic observations from the sonde data is around 5 m. Surface (10 m) wind speeds are estimated using measurements from a nadir-pointing stepped-frequency microwave radiometer (Uhlhorn et al. 2007). Sea surface temperature was measured using a Barnes (precision radiation thermometer) PRT-5 radiometer corrected for atmospheric radiation and absorption.

Turbulent fluxes of momentum, sensible heat, and humidity are calculated using the eddy correlation method for each flux run as follows:

$$\hat{\boldsymbol{\tau}} = \rho\,(-\overline{w'u'}\,\hat{\mathbf{i}} - \overline{w'v'}\,\hat{\mathbf{j}}), \tag{1}$$

$$H = \rho\, c_P \overline{w'\theta'}, \quad \text{and} \tag{2}$$

$$E = \rho\, L_v\, \overline{w'q'}, \tag{3}$$

respectively, where prime indicates turbulent fluctuations; u, v, w, θ, and q represent along-wind velocity, crosswind velocity, vertical velocity, potential temperature, and specific humidity, respectively; ρ represents the air density; c_p the specific heat at constant pressure; L_v the latent heat of vaporization; and an overbar the averages over the flux run.

Within a stepped descent, flux runs are identified based on stationarity of the measured quantities and flight parameters. Aircraft pitch and roll angles are checked to make sure that the aircraft was flying along a horizontal flight path. Any data with either the aircraft pitch or roll exceeding 5° (absolute value) are discarded. Further, legs with aircraft altitude variation greater than 30 m or heading variation greater than 20° are discarded. Examples of the 40-Hz time series of the aircraft altitude, attitude angles (pitch, roll, and heading), along-wind, crosswind, and vertical component wind velocities,

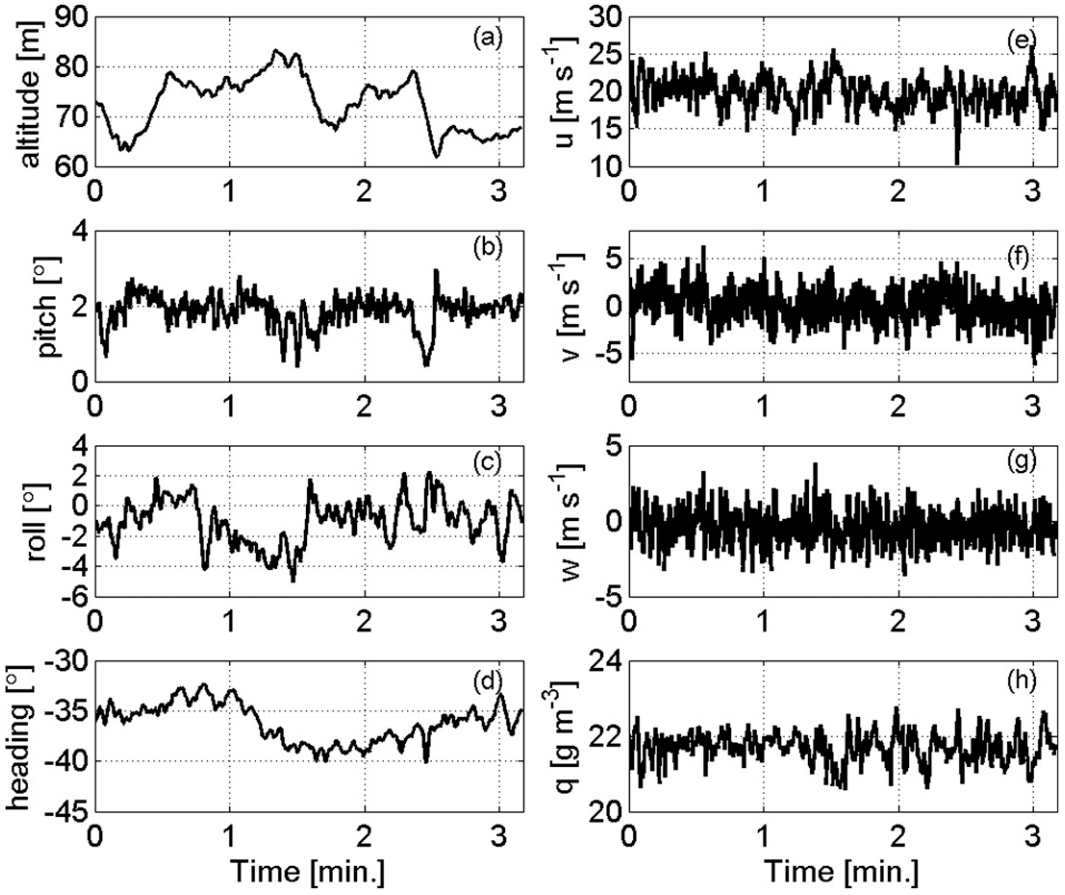

FIG. 1. Time series of (a) aircraft altitude, (b) pitch, (c) roll, (d) heading, (e) horizontal along-wind velocity, (f) horizontal crosswind velocity, (g) vertical velocity, and (h) absolute humidity for flux run 11 on 14 Sep 2003. All data are 40 Hz.

and humidity from a typical flux run are presented in Fig. 1.

Data quality assurance for individual flux legs includes inspection of the power spectra, cospectra, and cumulative summations of the cospectra or ogives of wind velocity components, potential temperature, and humidity (Friehe et al. 1991). The use of ogive curves when estimating fluxes provides insight into turbulent structure and the scales that contribute to turbulent transport. If the ogive curve approaches asymptotically a single value, then the stationarity condition is met, and the final value of the ogive represents the total covariance or flux. Figure 2 shows spectra and cospectra of the three components of the wind vector, potential temperature, and humidity for the flux run shown in Fig. 1. The ogives are also shown in Fig. 2. Note that here the ogives are summed from high frequency to low frequency. The flatness of the ogive curves at high and low frequencies indicates that the energy is well contained in the middle frequency range from 0.01 to 1 Hz.

In this study the turbulence structure of the hurricane boundary layer is investigated using data from 69 flux runs from eight boundary layer flights in four hurricanes during the 2003/04 Atlantic hurricane seasons. During 2003, 15 stepped descents from six flights provide data from Hurricanes Fabian and Isabel. There are a total of 52 flux runs in 2003, including 4 runs above the mixed layer. During the 2004 hurricane season, data from two flights are used in this analysis. These data are mostly from legs near or above the top of the mixed layer in Hurricanes Frances and Jeanne. There are a total of 17 flux runs taken in 2004. Data from regions with surface wind speeds between 16 and 30 m s^{-1} are used here to describe the vertical structure of fluxes and turbulence.

All the data in this study were collected with $|z_i/L| \ll 1$, indicating that the boundary layer is nearly neutral, where z_i is the thermodynamic boundary layer height (hereafter mixed layer depth), and L is the Obukhov length calculated from the measured fluxes. We define the mixed layer depth as the point where the

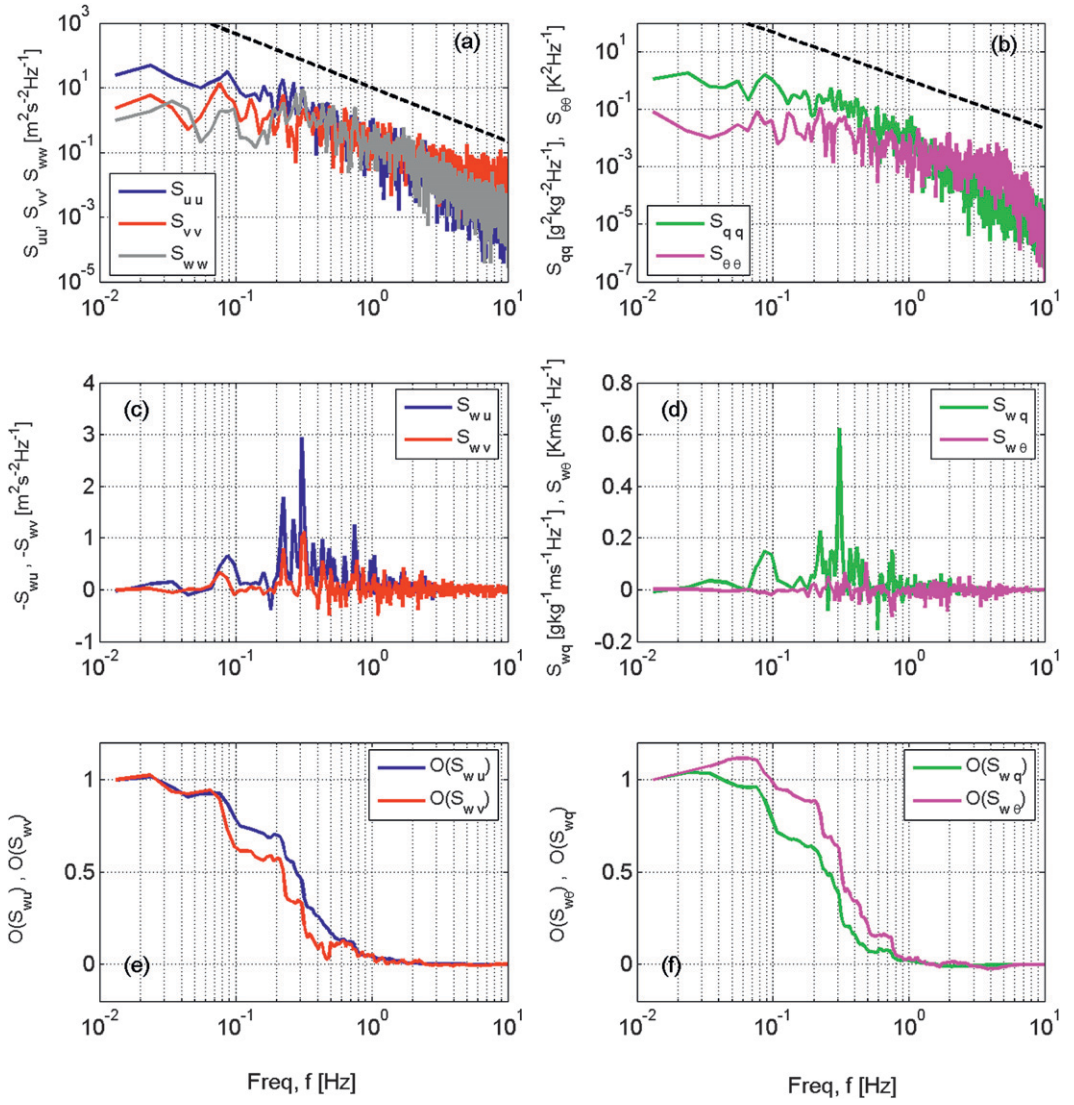

FIG. 2. Plots of (a) spectra of the three components of the wind vector (S_{uu}, S_{vv}, S_{ww}), (b) spectra of potential temperature ($S_{\theta\theta}$) and humidity (S_{qq}), (c) cospectra of uw and vw, (d) cospectra of θw and qw, (e) ogives of uw and vw, and (f) ogives of θw and qw. The ogives are normalized to unity. The black dashed lines in (a) and (b) show a −5/3 slope.

difference of the virtual potential temperature and the surface layer (nearly constant) virtual potential temperature is 0.5 K. Figure 3 shows the vertical profiles of wind speed, potential temperature, specific humidity, and virtual potential temperature from nine GPS dropsondes launched from N42RF flying above NOAA-43 during the stepped descents in Hurricanes Fabian and Isabel. Different colors represent profiles collected during different flights. Based on our above definition, the calculated mixed layer depth varies from 350 to 550 m with a mean value of around 400 m.

This height is similar to estimates found using other definitions of the boundary layer height. For instance, Anthes and Chang (1978) defined the boundary layer height as $[2K_m/(f + V_t/r)]^{1/2}$, where K_m is the eddy diffusivity, f is the Coriolis parameter, V_t is the tangential wind speed, and r is the radius to the storm center. Kepert (2001) and Kepert and Wang (2001) defined the hurricane boundary layer height as $\delta_0 = (2K_m/I)^{1/2}$, where I is the inertial instability that is defined as $I^2 = (f + 2V/r)(f + V/r + \partial V/\partial r)$, where V is the gradient wind speed. Kepert (2001) used $K_m = 50\ \mathrm{m^2\ s^{-1}}$, $\partial V/\partial r = xV/r$, and $x = -0.5$, following Gray and Shea (1973). Taking the data on 12 September 2003 as an example—$r \approx 120$ km, $V_t \approx 40\ \mathrm{m\ s^{-1}}$, and $V \approx 37\ \mathrm{m\ s^{-1}}$—the boundary layer heights estimated using the methods given by Anthes and Chang (1978) and Kepert (2001) are 510 and 520 m, respectively. Using our definition from the previous

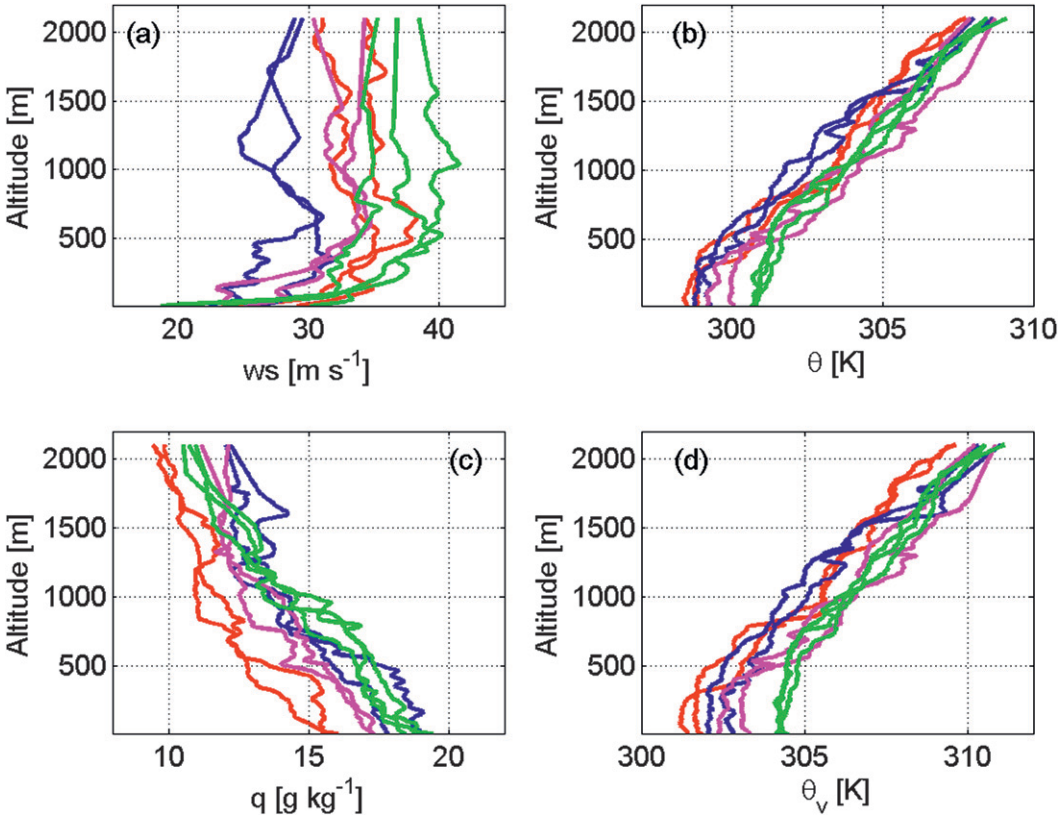

FIG. 3. Profiles of (a) wind speed, (b) potential temperature, (c) specific humidity, and (d) virtual potential temperature. Each curve represents a profile from a GPS sonde released from N42RF in the vicinity of a stepped descent. The colors red, blue, magenta, and green represent the flight days of 2, 3, 4, and 12 Sep 2003, respectively.

paragraph and dropsonde data from 12 September 2003, the mixed layer depth is 550 m.

3. Vertical profiles of turbulent fluxes

According to the similarity theory proposed by Monin and Obukhov (1954), surface layer scaling parameters for momentum, sensible heat, and humidity, respectively, can be derived from surface fluxes as follows:

$$u_* = (|\tau|_0/\rho)^{1/2}, \tag{4}$$

$$\theta_* = -[H_0/(\rho\, c_P)]\,/u_*, \quad \text{and} \tag{5}$$

$$q_* = -[E_0/(\rho\, L_v)]/u_*, \tag{6}$$

where the subscript 0 represents the value in the surface layer. We follow the typical convention for the assumed depth of the surface layer, the lowest 10% of the atmospheric boundary layer, wherein the fluxes are assumed to be constant.

Vertical profiles of the scaled momentum fluxes, where the measurement heights are scaled by the mixed layer depth, are shown in Fig. 4. The surface stress and u_* are estimated from the stepped descent momentum flux profiles as described in French et al. (2007). The horizontal bars represent one standard deviation around the mean in vertical bins. We use vertical bins of 0.25 z/z_i below the mixed layer depth and 0.5 z/z_i above it. The along-wind component of the vertical momentum flux shows a nearly linear profile, while the crosswind component is positive with a curvature that has the maximum value of around 0.5 u^2_* near the height of the mixed layer ($z/z_i = 1$). The shape of normalized momentum flux profiles is as expected, but the momentum fluxes, instead of vanishing at the top of the thermodynamic boundary layer as indicated from other observational studies, tend toward zero at nearly twice the mixed layer depth.

Figure 5a shows the vertical profile of the humidity fluxes. The humidity fluxes are mainly positive, indicating an upward transport of water vapor from the ocean surface. Statistical analyses on the slopes of the humidity profiles from all the stepped descents show that the humidity flux is invariant with height below 400 m (Drennan et al. 2007). Figure 5b shows the normalized vertical profiles of the nondimensional humidity fluxes.

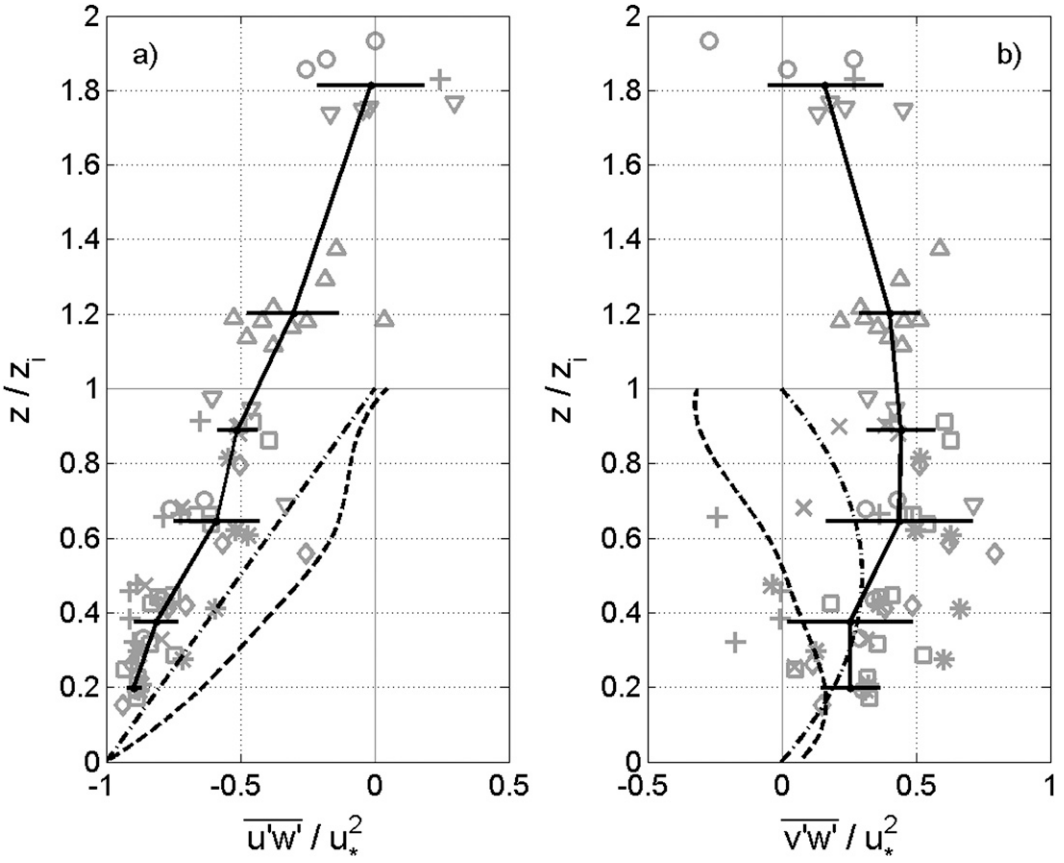

FIG. 4. Vertical profiles of the dimensionless covariances of the (a) along-wind and (b) crosswind components of velocity with vertical velocity. Black lines show the vertical bin averages and standard deviations. The symbols show data from different flight days: 2 Sep 2003 (○), 3 Sep 2003 (+), 4 Sep 2003 (×), 12 Sep 2003 (*), 13 Sep 2003 (◇), 14 Sep 2003 (□), 1 Sep 2004 (△), and 22 Sep 2004 (▽). The dashed line is from Nicholls and Readings (1979) and the dashed–dotted line is from Tjernström and Smedman (1993). The covariances have been normalized by the square of the surface friction velocity (u_*), and the altitude is normalized by the mixed layer depth z_i.

For the data from the stepped descent measurements, the mean value of the humidity flux below 400 m is used as the surface value for each stepped descent. For the 2004 data, when no flights below 400 m (i.e., no stepped descents) were made, surface fluxes are calculated using the bulk exchange coefficients developed by Drennan et al. (2007). Again, the black lines show the best fit by the vertically bin-averaged values. Consistent with the behavior noted above for individual stepped descents, the dimensionless humidity flux is nearly constant with height below the mixed layer depth and decreases with increasing height above the mixed layer. The humidity flux vanishes around $z/z_i = 1.9$, showing a similar behavior as the momentum flux profiles. Profiles of humidity flux from several earlier studies are also shown in Fig. 5b. Our results are qualitatively similar to those of Nicholls and Readings (1979) and DeCosmo et al. (1996), indicating the likely significance of entrainment of drier air from above the mixed layer.

Figure 6a shows the vertical profile of sensible heat flux. In general, the sensible heat fluxes are very small throughout the boundary layer. We found 85% of the data to have negative sensible heat flux, indicating the sensible heat is transported downward for much of the time. The extrapolated surface fluxes correlated very well with stability calculated from the air–sea temperature difference (Zhang et al. 2008). However, using the extrapolated surface sensible heat fluxes or $-u_*\theta_*$ to scale the sensible heat flux profile gives a large scatter, as shown in Fig. 6b, because the surface values of sensible heat flux are relatively small compared to those measured at the flight level.

4. Vertical profiles of variances

Studies of velocity, temperature, and humidity variances in the atmospheric boundary layer provide a direct test of similarity predictions as well as indirect estimates

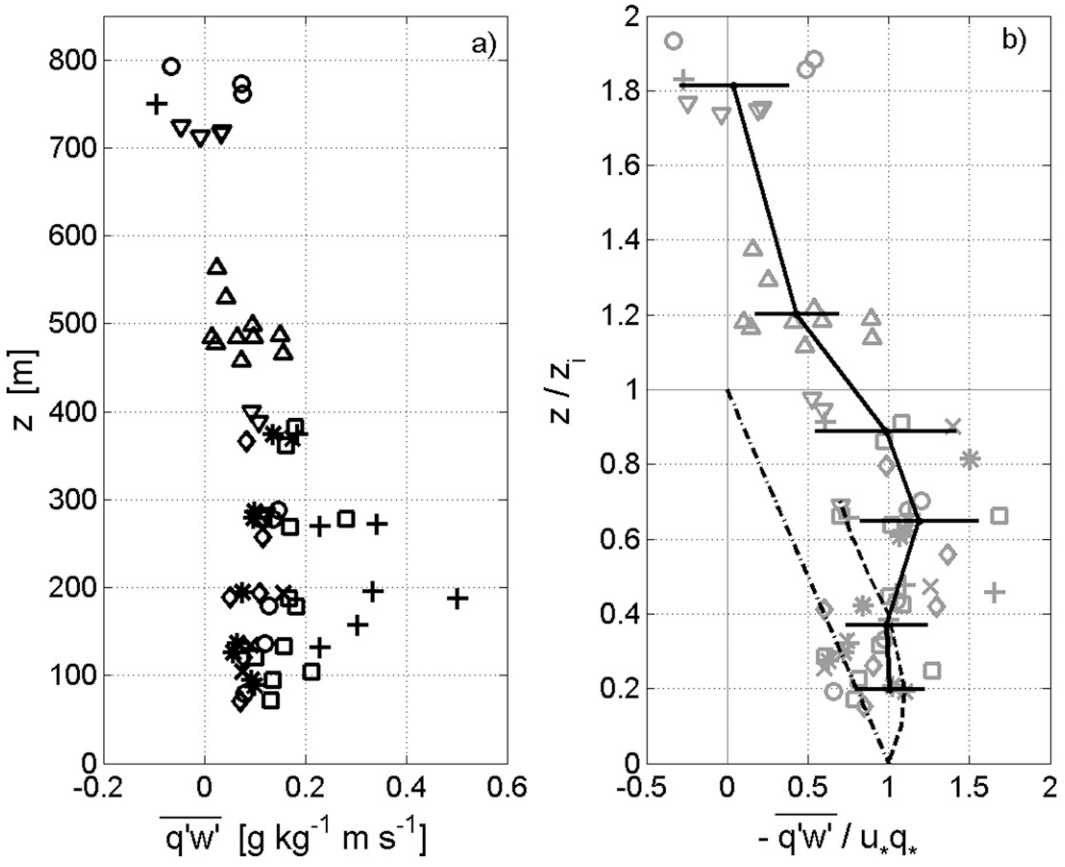

FIG. 5. Vertical profiles of the (a) covariances of specific humidity with vertical velocity and (b) dimensionless covariances with height normalized by the mixed layer depth. Symbols and lines are the same as in Fig. 4.

of vertical fluxes. In the surface layer, nondimensional variances or standard deviations normalized by the surface layer scaling parameters are expected to be universal functions of z/L if Monin–Obukhov scaling is correct (Stull 1988). Higher up in the boundary layer, both surface layer scaling and mixed layer scaling are expected to be important (Nicholls and Readings 1979).

The dimensionless standard deviations of along-wind and crosswind components of wind velocity versus height normalized by the mixed layer depth z_i are shown in Figures 7a and b, respectively. Figure 8a shows the normalized dimensionless standard deviation of vertical wind velocity. Previous turbulence measurements by Nicholls and Readings (1979) and Tjernström and Smedman (1993) are also shown. The standard deviation of the along-wind velocity component shows a slight decrease with the increasing height, while that of the crosswind component stays relatively invariant with the height. The values of $\sigma_{u,v}/u_*$ are similar to those of the ''slightly convective'' case of Nicholls and Readings (1979). The vertical velocity variance shown in Fig. 8a exhibits nearly constant behavior with height within the mixed layer, but it decreases with height above the mixed layer.

Surface layer similarity theory expressions for $\sigma_{u,v}/u_*$ under neutral conditions, summarized by Stull (1988) from studies by Wyngaard and Coté (1971), Panofsky et al. (1977), Nicholls and Readings (1979), Smith (1980), Grant (1986), and Sorbjan (1986) are given by

$$\frac{\sigma_u}{u_*} = 2.5 \pm 0.04 \quad \text{and} \tag{7}$$

$$\frac{\sigma_v}{u_*} = 2.0 \pm 0.36. \tag{8}$$

The surface layer similarity theory expression of σ_w/u_*, essentially derived from the Kansas data (Businger et al. 1971) then reexamined and refined through comparisons with other observations by Högström (1988), is given by

$$\frac{\sigma_w}{u_*} = \begin{cases} 1.25\,(1 + 3|z/L|)^{1/3}, & -2 \le z/L \le 0 \\ 1.25\,(1 + 0.2z/L)^2, & 0 \le z/L \le 1 \end{cases}. \tag{9}$$

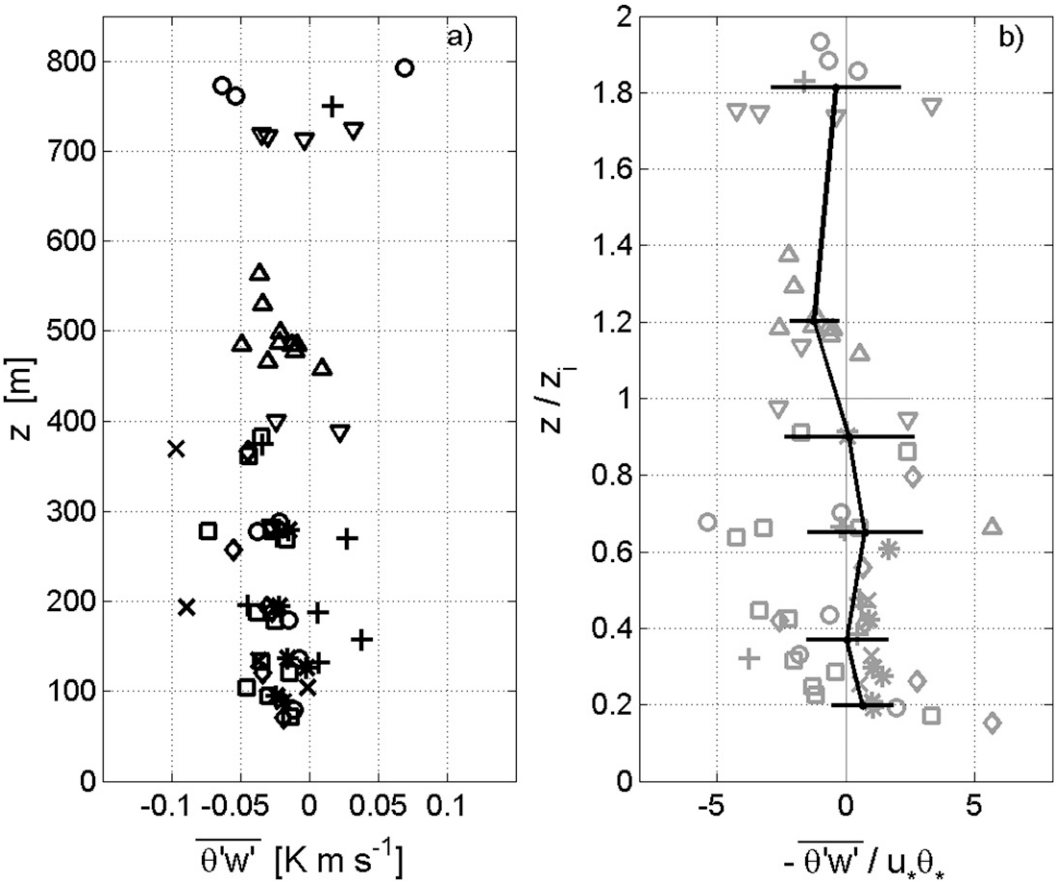

FIG. 6. Vertical profiles of the (a) covariances of potential temperature and vertical velocity, and (b) dimensionless covariances with height normalized by the mixed layer depth. Symbols are the same as in Fig. 4.

In this study, the extrapolated surface layer values of the scaled variances for the CBLAST data are as follows:

$$\frac{\sigma_u}{u_*} = 2.7 \pm 0.2, \quad \frac{\sigma_v}{u_*} = 3 \pm 0.2, \quad \text{and} \quad \frac{\sigma_w}{u_*} = 1.25 \pm 0.25. \tag{10}$$

The value of σ_v/u_* is significantly higher than previous values (8). However, σ_u/u_* and σ_w/u_* derived from the CBLAST data are comparable to those calculated from (7) and (9), respectively.

The vertical profiles of the standard deviation of specific humidity scaled by q_* are shown in Fig. 8b. The scatter is substantially larger here than in the variance plots for wind velocity. The dimensionless standard deviation of humidity shows a smaller variation with height within the mixed layer that is consistent with the humidity flux profiles. Although the scatter is larger in our data, the value of σ_q/q_* extrapolated to the surface is comparable to those reported by Nicholls and Readings (1979).

5. Turbulent kinetic energy budget

The TKE budget of horizontally homogeneous turbulence can be given by

$$\frac{De}{Dt} = -\overline{u'w'}\frac{\partial \overline{u}}{\partial z} - \overline{v'w'}\frac{\partial \overline{v}}{\partial z} + (g/\overline{\theta})\overline{w'\theta'} + 0.61g\overline{w'q'} - \frac{\partial \overline{w'e}}{\partial z} - \frac{1}{\rho}\frac{\partial \overline{w'p'}}{\partial z} - \varepsilon, \tag{11}$$

where e is the TKE, defined as $e = \frac{1}{2}(u'^2 + v'^2 + w'^2)^{1/2}$, and ε is the dissipation rate of turbulent kinetic energy. The left-hand side of (11) is the total derivative and therefore includes the local change and the horizontal advection terms $De/Dt = \partial e/\partial t + \overline{u}(\partial e/\partial x) + \overline{v}(\partial e/\partial y)$. On the right-hand side, the first and second terms together are the shear production, the third and fourth terms together are the buoyancy production, the fifth term is the turbulent transport of TKE, the sixth term is the pressure transport, and the last term is the dissipation. An examination of the terms in the turbulent kinetic

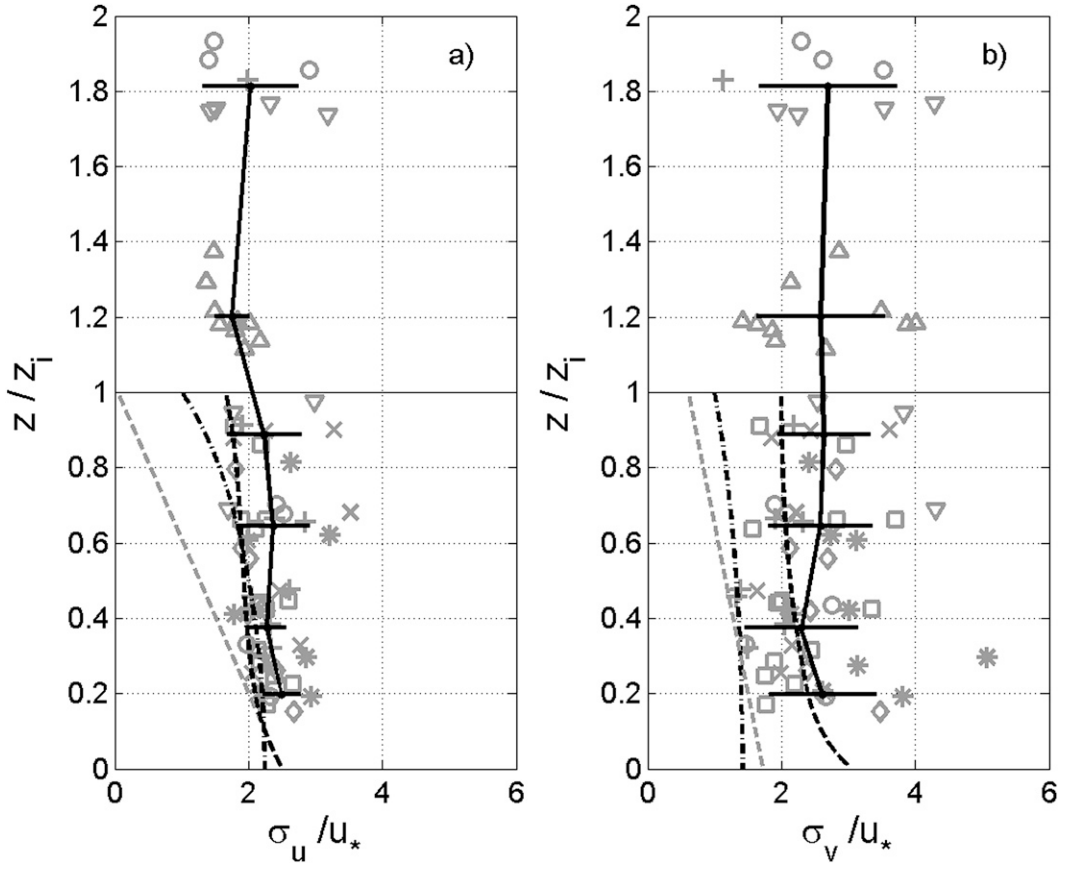

FIG. 7. Vertical profiles of the dimensionless standard deviations of (a) the along-wind and (b) the crosswind components of the wind velocity with height normalized by the mixed layer depth. The dashed lines are from Nicholls and Readings (1979) for data taken over the ocean at moderate wind speeds. The black dashed line represents data in slightly convective conditions, while the gray dashed line represents data in nearly neutral conditions. The dashed–dotted line is from Tjernström and Smedman (1993) for data in nearly neutral conditions over the coastal ocean. Symbols and solid lines are as in Fig. 4.

energy equation aids our understanding of the nature of turbulent production and destruction in the boundary layer. The measurements made during CBLAST provide estimates of most of the terms in the kinetic energy budget. Terms that cannot be measured are grouped together into a residual term, $R = De/Dt + (1/\rho)(\partial\overline{w'p'}/\partial z)$.

The dissipation term is estimated from the spectral density of the longitudinal velocity component in the high-frequency range from 2 to 4 Hz, where the velocity components exhibit a $f^{-5/3}$ power law in their spectra, the so-called inertial subrange. The dissipation of TKE is given by

$$\varepsilon = \alpha_u^{-3/2}\frac{2\pi f}{U}[fS_{uu}(f)]^{3/2}, \tag{12}$$

where α_u is the one-dimensional Kolmogorov constant, U is the airspeed relative to the aircraft, and S_{uu} is the power-spectral density of the horizontal along-wind wind speed. In this study, we use $\alpha_u = 0.5$, following Sreenivasan (1995).

The buoyancy production consists of two parts: one part is due to the sensible heat and the other due to the humidity flux. Both of these are directly measured. Since the mean wind gradient cannot be accurately determined from the aircraft wind measurements, the first two terms on the right-hand side of (11) are not directly accessible. The shear production term is estimated by $u_*^3/\kappa z$, a relation which, strictly speaking, is only valid under neutral conditions. Here, $\kappa = 0.4$ is the von Kármán constant.

In this study the TKE transport term is directly measured. However, the pressure transport term is not measured. We group it together with other unmeasured terms (i.e., the rate of change of TKE and the advection of TKE) as a combined residual term.

Figure 9 shows the TKE budget of the boundary layer in the rain-free region between the rainbands. The TKE

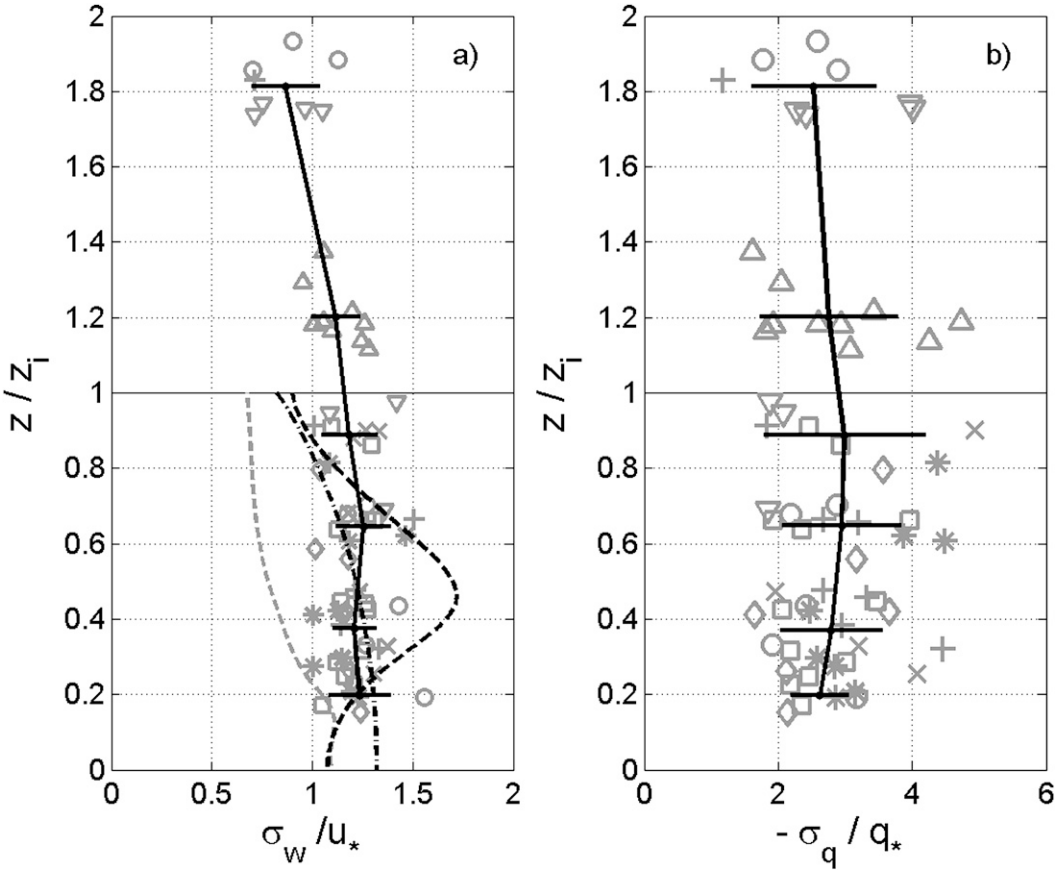

FIG. 8. Vertical profiles of the dimensionless standard deviations of (a) vertical wind velocity and (b) specific humidity with height normalized by the mixed layer depth. Symbols and lines are as in Fig. 7.

budget is primarily dominated by the shear production, whereas the buoyancy is nearly zero, confirming the near-neutrality of the boundary layer. It is also found that the dissipation term is significantly larger than the shear production. The pressure transport term is usually assumed to be small (Donelan 1990), especially at these heights above the surface, though Högström's (1990) results indicate that this is not always the case; therefore, refer to the discussion below. We speculate that the unmeasured advection term is an important source for the turbulent kinetic energy in the hurricane boundary layer.

6. Discussion and conclusions

In this study, we present the first in situ aircraft investigation of the turbulence structure of the hurricane boundary layer, and the first estimate of the turbulent kinetic energy budget for the atmospheric boundary layer between the outer rainbands. The vertical structure of turbulence and fluxes are presented. The along-wind component of momentum flux decreases linearly with height, while the crosswind component of momentum flux has the expected Northern Hemisphere curvature with a maximum value at the height of the mixed layer. The humidity flux is nearly constant with height within the mixed layer and decreases with increasing height above that. The sensible heat flux is mostly negative for the entire boundary layer, showing downward transport of heat from above. The dimensionless variances of the horizontal crosswind component of wind velocity are significantly larger than those reported from previous studies, but the dimensionless variances of the vertical wind velocity and specific humidity agree well with previous results.

Prior to this study, there is only one experiment with turbulent flux measurements in the boundary layer of a tropical cyclone, conducted by Moss and Merceret (1976) and also by Moss (1978), who investigated turbulent properties of boundary layer in the periphery of tropical storm Eloise in 1975. They used a hot-film anemometer to measure the high-frequency along-wind velocity component and a gust probe to measure the lateral and vertical wind speed components, and computed momentum fluxes during seven level legs at different

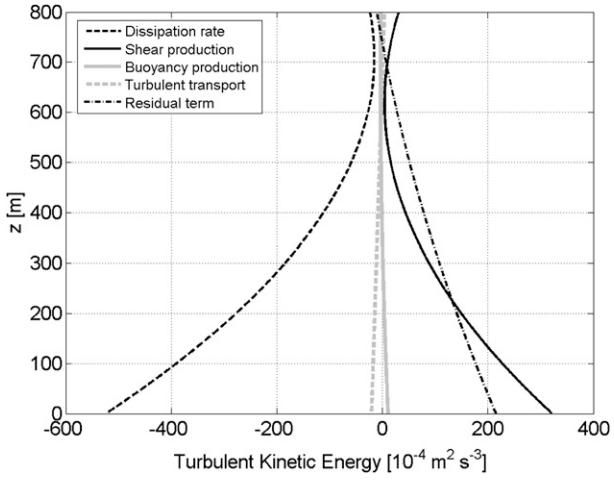

FIG. 9. Vertical profiles of shear production, buoyancy, turbulent transport, rate of dissipation, and the residual term of the TKE budget.

altitudes from 85 to 1213 m. Moss (1978) found that the momentum flux vanishes at the top of the mixed layer, defined by the middle of the inversion layer from the potential temperature profile (i.e., roughly our z_i). This is consistent with measurements outside of tropical cyclones (e.g., Nicholls and Readings 1979) but very different from what we found here. In numerical models, the boundary layer height is usually defined from the virtual potential temperature profile as the height of the lowest inversion layer, where turbulent fluxes typically vanish. Use of this definition may cause biased simulation of boundary layer flux profiles for the region between the outer rainbands based on the CBLAST data.

Measurements of terms in the TKE budget imply that the major source, the shear production, is dissipated locally with the buoyancy and turbulent transport terms being relatively unimportant. The TKE budget conducted in this study indicates that the dissipation term is greater than the production terms by 50% in the surface layer extrapolated from above. Bister and Emanuel (1998) discuss the possibility that viscous dissipation of turbulent kinetic energy in the surface layer could be an additional heat source for tropical cyclones. They also suggest that maximum dissipative heating would tend to occur in the high-wind regime near and under the eyewall. Our results show that the viscous dissipation is significantly stronger than the shear production in the region between the outer rainbands.

The terms in the TKE budget have been evaluated in many experiments in the atmospheric boundary layer or surface layer in low-to-moderate winds (i.e., nonhurricane conditions). Lenschow (1970) investigated the terms in the TKE budget in a very unstable boundary layer over land and found that the buoyancy production is the main source for the TKE generation. Nicholls (1985) conducted the TKE budget for the nearly neutral and slightly unstable midlatitude atmospheric boundary layers over the ocean, and they found shear production to be the main source for TKE generation. Although the mechanisms of generating turbulence in different types of boundary layer differ significantly, the dominant production term and the dissipation term in the TKE budget are generally nearly balanced (i.e., Lenschow 1970; Nicholls 1985, among others). However, there are also cases in which they are not balanced. For instance, Högström (1990) found that dissipation of TKE at neutral stability was greater than production by 24% in the surface layer over a terrestrial site. He suggested that this discrepancy may be due to the dissipation of ''inactive turbulence,'' which is not produced by shear in the surface layer but rather by processes at the top of the boundary layer.

However, we hypothesize the stronger imbalance between the dissipation and shear production in this study results from the nonlinear horizontal advection terms in the TKE budget, which were not measured but should be very important for the local budget of turbulent kinetic energy in the hurricane boundary layer. One of the unique features of the hurricane boundary layer is the decoupling of the primary circulation and the secondary circulation. Surface friction–induced imbalance between the pressure gradient, Coriolis force, and centrifugal force drives inflow into the boundary layer, thereby inducing a secondary circulation in the vortex (Smith 1968). The strong inflow may be the main cause of the advection of TKE toward the center of the storm.

The importance of the inflow layer in tropical cyclone dynamics can be seen in Fig. 10, which shows a schematic conceptual model for the hurricane boundary layer height for the region between the outer rainbands. Here, h represents the boundary layer height defined using the momentum flux profile (i.e., the height where turbulent mixing goes to zero); h_{inflow} represents the inflow layer height defined using the radial wind velocity (V_r) profile as the height at which $V_r = 0$; and h_{Vtmax} is the height of the maximum tangential wind speed. As mentioned earlier, z_i is the mixed layer depth defined using the virtual potential temperature profile. Note that all these boundary layer height scales are calculated using the CBLAST data. The vertical profiles of virtual potential temperature and radial and tangential wind velocities plotted in Fig. 10 are the mean profiles derived from nine GPS dropsondes that were deployed close (in space and time) to the NOAA-43 stepped descents. Individual profiles were plotted in Fig. 3. There is a clear separation of boundary layers defined thermodynamically and mechanically. Turbulent fluxes

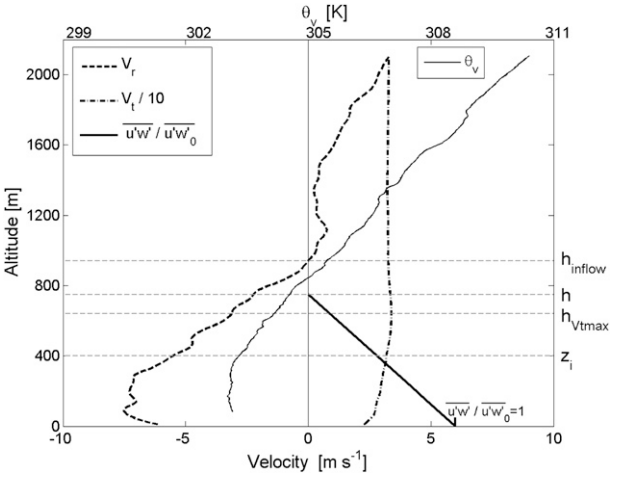

FIG. 10. Height scales of the hurricane boundary layer between outer rainbands. Abbreviations are defined in the text. The vertical profiles of virtual potential temperature and radial wind and tangential wind velocity are the mean profiles derived from the nine GPS dropsondes plotted in Fig. 3. The momentum flux profile is based on Fig. 4.

decrease to zero, not at the mixed layer depth as is typical in most boundary layers but at a height between that of the maximum tangential wind speed and the inflow layer height. This indicates the complicated energy transport processes in the boundary layer of major hurricanes. Apparently turbulent transport processes through turbulent eddies in the forms of momentum and enthalpy flux cannot be fully explained only by surface processes (or bulk exchange coefficients). Other processes such as turbulent mixing, advection, and entrainment processes near the top of the boundary layer are also important. In particular, horizontal advection cannot be neglected, as shown by the turbulent kinetic energy budget.

Our results emphasize the importance of understanding the turbulence structure within the inflow layer, crucial to the parameterization of the hurricane boundary layer. The results presented in this study provide a valuable resource for the evaluation of boundary layer parameterization schemes used in hurricane models.

Acknowledgments. This work is supported through ONR's CBLAST-Hurricane program (Grant N00014-01-F-0090) and NOAA's OAR/USWR program as well as through NOAA/OAR laboratories AOML and ARL. We would like to acknowledge, in particular, Simon Chang and Carl Friehe (ONR) for their efforts in planning and organizing the multiyear CBLAST program, John Gaynor (OAR/USWRP) for his support, the CBLAST co-PIs and the flight and support crews of NOAA-43. We appreciate comments from Frank Marks and Sim Aberson. The first author also acknowledges support from the National Research Council's Research Associateship Program of the National Academies, administered in cooperation with NOAA/AOML's Hurricane Research Division.

REFERENCES

Anthes, R. A., and S. W. Chang, 1978: Response of the hurricane boundary layer to changes of sea surface temperature in a numerical model. *J. Atmos. Sci.,* **35,** 1240–1255.

Bister, M., and K. A. Emanuel, 1998: Dissipative heating and hurricane intensity. *Meteor. Atmos. Phys.,* **65,** 233–240.

Black, P. G., and Coauthors, 2007: Air–sea exchange in hurricanes: Synthesis of observations from the Coupled Boundary Layer Air–Sea Transfer experiment. *Bull. Amer. Meteor. Soc.,* **88,** 357–374.

Braun, S. A., and W.-K. Tao, 2000: Sensitivity of high-resolution simulations of Hurricane Bob (1991) to planetary boundary layer parameterizations. *Mon. Wea. Rev.,* **128,** 3941–3961.

Businger, J. A., J. C. Wyngaard, Y. K. Izumi, and E. F. Bradley, 1971: Flux-profile relationships in the atmosphere surface layer. *J. Atmos. Sci.,* **28,** 181–189.

Chen, S. S., J. F. Price, W. Zhao, M. A. Donelan, and E. J. Walsh, 2007: The CBLAST-Hurricane program and the next-generation fully coupled atmosphere–wave–ocean models for hurricane research and prediction. *Bull. Amer. Meteor. Soc.,* **88,** 311–317.

DeCosmo, J., K. B. Katsaros, S. D. Smith, R. J. Anderson, W. A. Oost, K. Bumke, and H. Chadwick, 1996: Air-sea exchange of water vapor and sensible heat: The humidity exchange over the sea (HEXOS) results. *J. Geophys. Res.,* **101,** 12 001–12 016.

Donelan, M. A., 1990: Air-sea interaction. *Ocean Engineering Science*, B. Le Méhauté and D. M. Hanes, Eds., Vol. 9, *The Sea: Ideas and Observations on Progress in the Study of the Seas,* John Wiley and Sons, 239–292.

Drennan, W. M., J. A. Zhang, J. R. French, C. McCormick, and P. G. Black, 2007: Turbulent fluxes in the hurricane boundary layer. Part II: Latent heat flux. *J. Atmos. Sci.,* **64,** 1103–1115.

Emanuel, K. A., 1995: Sensitivity of tropical cyclones to surface exchange coefficients and a revised steady-state model incorporating eye dynamics. *J. Atmos. Sci.,* **52,** 3969–3976.

French, J. R., W. M. Drennan, J. A. Zhang, and P. G. Black, 2007: Turbulent fluxes in the hurricane boundary layer. Part I: Momentum flux. *J. Atmos. Sci.,* **64,** 1089–1102.

Friehe, C. A., and D. Khelif, 1992: Fast-response aircraft temperature sensors. *J. Atmos. Oceanic Technol.,* **9,** 784–795.

——, and Coauthors, 1991: Air-sea fluxes and surface turbulence around a sea surface temperature front. *J. Geophys. Res.,* **96,** 8593–8609.

Grant, A. L. M., 1986: Observations of boundary layer structure made during the 1981 KONTUR experiment. *Quart. J. Roy. Meteor. Soc.,* **112,** 825–841.

Gray, W. M., and D. S. Shea, 1973: The hurricane's inner core region. Part II: Thermal stability and dynamics characteristics. *J. Atmos. Sci.,* **30,** 1565–1576.

Högström, U., 1988: Nondimensional wind and temperature profiles in the atmospheric surface layer: A reevaluation. *Bound.-Layer Meteor.,* **42,** 55–78.

——, 1990: Analysis of turbulence structure in the surface layer with a modified similarity formulation for near neutral conditions. *J. Atmos. Sci.,* **47,** 1949–1972.

Kepert, J. D., 2001: The dynamics of boundary layer jets within the tropical cyclone core. Part I: Linear theory. *J. Atmos. Sci.,* **58,** 2469–2484.

——, 2006: Observed boundary layer wind structure and balance in the hurricane core. Part I: Hurricane Georges. *J. Atmos. Sci.,* **63,** 2169–2192.

——, and Y. Wang, 2001: The dynamics of boundary layer jets within the tropical cyclone core. Part II: Nonlinear enhancement. *J. Atmos. Sci.,* **58,** 2485–2501.

Khelif, D., S. P. Burns, and C. A. Friehe, 1999: Improved wind measurements on research aircraft. *J. Atmos. Oceanic Technol.,* **16,** 860–875.

Lenschow, D. H., 1970: Airplane measurements of planetary boundary layer structure. *J. Appl. Meteor.,* **9,** 874–884.

Monin, A. S., and A. M. Obukhov, 1954: Basic laws of turbulent mixing in the ground layer of the atmosphere. *Tr. Geofiz. Inst., Akad. Nauk SSSR,* **151,** 163–187.

Morrison, I., S. Businger, F. Marks, P. Dodge, and J. A. Businger, 2005: An observational case for the prevalence of roll vortices in the hurricane boundary layer. *J. Atmos. Sci.,* **62,** 2662–2673.

Moss, M. S., 1978: Low-level turbulence structure in the vicinity of a hurricane. *Mon. Wea. Rev.,* **106,** 841–849.

——, and F. J. Merceret, 1976: A note on several low-layer features of Hurricane Eloise (1975). *Mon. Wea. Rev.,* **104,** 967–971.

——, and ——, 1977: A comparison of velocity spectra from hot film anemometer and gust-probe measurements. *J. Appl. Meteor.,* **16,** 319–320.

Nicholls, S., 1985: Aircraft observations of the Ekman layer during the Joint Air-Sea Interaction Experiment. *Quart. J. Roy. Meteor. Soc.,* **111,** 391–426.

——, and C. J. Readings, 1979: Aircraft observations of the structure of the lower boundary layer over the sea. *Quart. J. Roy. Meteor. Soc.,* **105,** 785–802.

Panofsky, H. A., H. Tennekes, D. H. Lenschow, and J. C. Wyngaard, 1977: The characteristics of turbulent velocity components in the surface layer under convective conditions. *Bound.-Layer Meteor.,* **11,** 355–361.

Powell, M. D., 1990a: Boundary layer structure and dynamics in outer hurricane rainbands. Part I: Mesoscale rainfall and kinematic structure. *Mon. Wea. Rev.,* **118,** 891–917.

——, 1990b: Boundary layer structure and dynamics in outer hurricane rainbands. Part II: Downdraft modification and mixed layer recovery. *Mon. Wea. Rev.,* **118,** 918–938.

Smith, R. K., 1968: The surface layer of a hurricane. *Tellus,* **20,** 473–484.

——, M. T. Montgomery, and S. Vogl, 2008: A critique of Emanuel's hurricane model and potential intensity theory. *Quart. J. Roy. Meteor. Soc.,* **134,** 551–561.

Smith, S. D., 1980: Wind stress and heat flux over the ocean in gale force winds. *J. Phys. Oceanogr.,* **10,** 709–726.

Sorbjan, Z., 1986: On the similarity in the atmospheric boundary layer. *Bound.-Layer Meteor.,* **34,** 377–397.

Sreenivasan, K. R., 1995: On the universality of the Kolmogorov constant. *Phys. Fluids,* **7,** 2778–2784.

Stull, R. B., 1988: *An Introduction to Boundary Layer Meteorology*. Atmospheric and Oceanographic Sciences Library, Vol. 13, Kluwer Academic, 670 pp.

Tjernström, M., and A.-S. Smedman, 1993: The vertical structure of the coastal marine atmospheric boundary layer. *J. Geophys. Res.,* **98,** 4809–4826.

Uhlhorn, E. W., P. G. Black, J. L. Franklin, M. Goodberlet, J. Carswell, and A. S. Goldstein, 2007: Hurricane surface wind measurements from an operational stepped frequency microwave radiometer. *Mon. Wea. Rev.,* **135,** 3070–3085.

Wurman, J., and J. Winslow, 1998: Intense sub-kilometer boundary layer rolls in Hurricane Fran. *Science,* **280,** 555–557.

Wyngaard, J. C., and O. R. Coté, 1971: Budgets of turbulent kinetic energy and temperature variance in the atmospheric surface layer. *J. Atmos. Sci.,* **28,** 1171–1182.

Zhang, J. A., P. G. Black, J. R. French, and W. M. Drennan, 2008: First direct measurements of enthalpy flux in the hurricane boundary layer: The CBLAST results. *Geophys. Res. Lett.,* **35,** L14813, doi:10.1029/2008GL034374.